Two-phase swirling flow in the barrel of a steam separator

MIKA Takeshi, MATSUBAYASHI Toshiki, HOSOKAWA Shigeo, and TOMIYAMA Akio

Department of Mechanical Engineering, Faculty of Engineering, Kobe University, 1-1 Rokkodai, Nada, Kobe, 657-8501 Japan (tomiyama@mech.kobe-u.ac.jp)

Abstract: A downscaled model of a steam separator was used to understand the characteristics of swirling flow after passing through the first pick-off ring (POR). Main conclusions obtained were as follows: (1) At high liquid volume fluxes, many droplets are entrained in the gas core at the downstream edge of the POR. The liquid film thickness above the POR gradually increases due to deposition and accumulation of droplets. (2) At low liquid volume fluxes, water accumulates just behind the POR. (3) A smooth rear edge on the first POR reduces the entrainment of droplets and increases separation performance at the second POR especially under high liquid volume flux conditions.

Keyword: steam separator; two-phase flow; swirling flow; pick-off ring; boiling water reactor

1 Introduction

Boiling water reactors (BWRs) are equipped with steam separators for splitting a two-phase mixture into steam and water before feeding the steam to dryers and turbines. The steam separator consists of a standpipe, a diffuser with a swirler, and a barrel with several pick-off-rings (PORs). The swirler's stationary vanes apply large centrifugal force to the steam-water two-phase flow, and most of the water in the barrel rapidly migrates toward the barrel wall. An annular swirling flow with few droplets in the gas core is, therefore, formed in the barrel. The liquid film flow and the gas core flow are separated by the PORs.

Sufficient information about characteristics of two-phase swirling flow in the barrel is required for improving separator performance. However, knowledge of annular swirling flow in the separator is still in its infancy [1, 2]. Hence, in our previous study [3, 4] we focused on two-phase swirling flow in the upstream region of the first POR, and measured flow patterns, liquid film thickness, droplet diameters and separation performance (defined as the ratio of the separated liquid flow rate to the total liquid flow rate) in air-water annular swirling flows in a one-fifth scale model of the steam separator. This earlier work enabled us to understand some of the key characteristics of swirling flow and to establish an experimental database for verification of numerical methods. We also experimentally investigated the effects of gap size in the POR [5] and swirler vane shape [6] on separation performance.

The purpose of the present study is to understand characteristics of swirling flow after the steam-liquid mixture has passed through the first POR. Experiments were carried out at atmospheric pressure and room temperature using a downscaled model of a steam separator in which a simulated POR was installed. Flow patterns, distributions of liquid film thickness and separation performances were measured for a wide range of gas and liquid volume fluxes to understand the effects of the simulated POR on the flow. We also designed an improved POR and examined its performance.

2 Experiments

2.1 Experimental setup

Figure 1 shows the experimental apparatus, which consists of the upper tank, barrel (inner diameter D = 40 **mm**, length L = 240 **mm**), diffuser (L = 33 **mm**), standpipe (D = 30 **mm**, L = 200 **mm**), plenum (D = 60 **mm**, L = 300 **mm**), gas-liquid mixing section, water supply system and air supply system. The barrel, diffuser and standpipe were made of transparent acrylic resin for observation and optical measurements of the two-phase flow. The size was about one-fifth of an actual steam separator used in a BWR. Air was supplied to the mixing section from an oil-free compressor (Oil-free Scroll compressor, SRL-11P6AI,

Received date: March 3, 2012
(Revised date: May 23, 2012)

Hitachi Ltd.), through a regulator (R600-20, CKD Ltd.) and flowmeter (FLT-N, Flowcell, Ltd.). Tap water at room temperature (293**K**) was supplied to the mixing section using a magnetic-drive pump (MD-40RX, Iwaki, Ltd.) through a flowmeter. The two-phase flow was formed in the mixing section and flowed in the upward direction through the plenum, standpipe, diffuser, and barrel. The shape of the swirler is shown in Fig. 2.

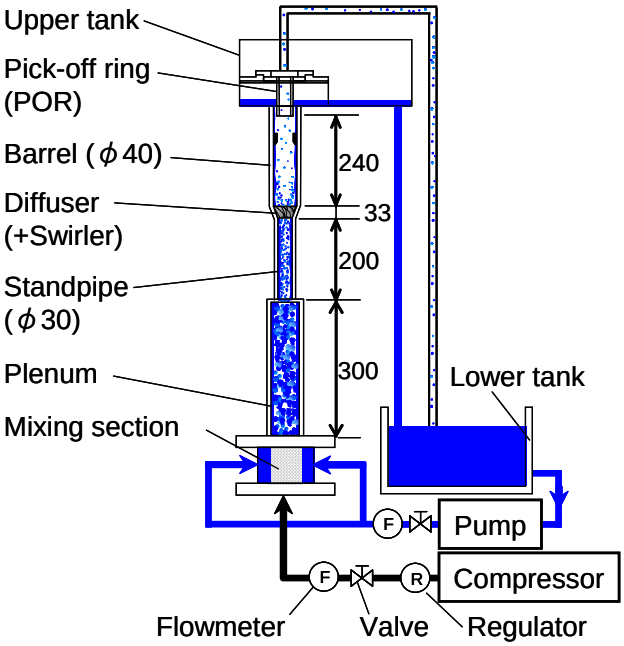

Fig. 1 Experimental setup.

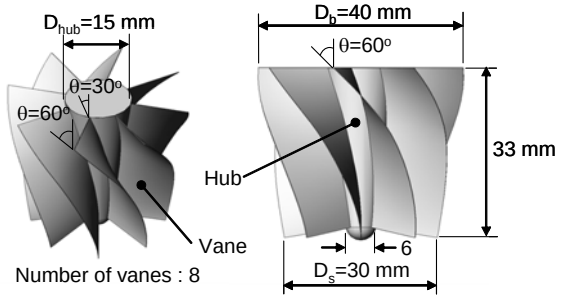

Fig. 2 Swirler.

Figure 3 shows schematics of the flows in the barrels of the model separators used in our previous study [5,6] and the present study. In an actual steam separator, the liquid film flow and the gas core flow are separated by the first POR as shown in Fig. 3 (a). The unseparated liquid, droplets and gas flow into the downstream region of the first POR. In this study, we installed a ring-shaped obstacle in the barrel to simulate the first POR as shown in Fig. 3 (b). The simulated POR had a slope in its front in order to minimize the disturbance to the liquid film at the front edge. The inner diameter of the simulated POR was 32 mm.

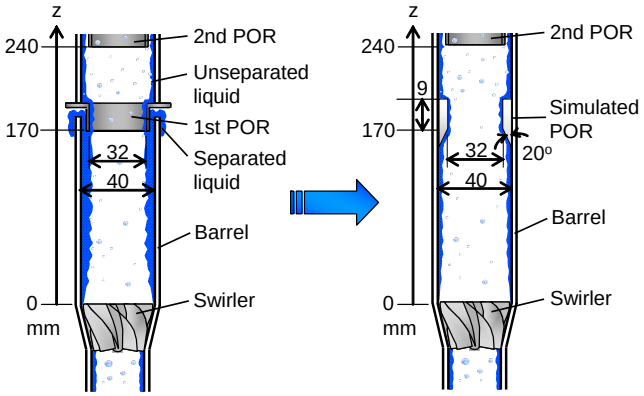

(a) Model separator used in our previous study[5,6] (b) The present model separator with simulated 1st POR

Fig. 3 Schematics of flows in barrels.

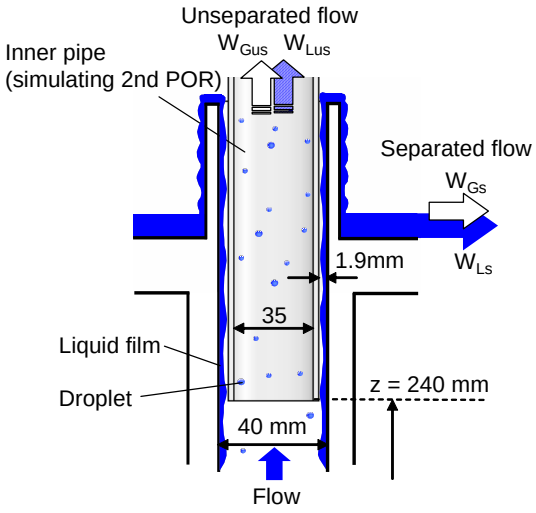

Fig. 4 Separation section.

Figure 4 shows the upper part of the barrel. At the exit of the barrel the liquid film was separated from the gas core flow by the inner pipe, which corresponds to the second POR. The lower end of the inner pipe was located at z = 240 **mm**, where z is the distance from the bottom of the barrel. The gap between the barrel wall and the outer wall of the inner pipe was 1.9 **mm**, and the wall thickness and inner diameter of the inner pipe were 0.6 and 35.0 **mm**, respectively. Most of the liquid film flowed through the gap, while most of the air and droplets flowed through the inner pipe. The separated liquid and droplets were returned to the lower tank through independent pipelines.

2.2 Experimental conditions and measurements

Experimental conditions were determined so as to cover the typical operating conditions of a BWR separator. The quality x, the gas and liquid volume fluxes, J_G and J_L, corresponding to the nominal operating conditions of the Hyper ABWR[7] are 0.18, 14.6 **m/s**, and 0.080 **m/s**, respectively[3]. Since the liquid volume flux in the downstream region of the first POR is to be lower than that in the upstream region of the first POR due to the separation of liquid film at the first POR, the present experiments were carried out under the conditions of J_G = 8.0 – 24.1 **m/s** and J_L = 0.005 – 0.080 **m/s**. Note that typical values of J_G and J_L downstream of the first POR under normal operating conditions have been estimated as 14.6 and 0.031 **m/s**, respectively, from preliminary experiments.

Flow patterns in the barrel were observed using a high-speed video camera (Redlake Motion Pro HS-1, frame rate = 4000 **frame/s**, exposure time = 100 **μs**). The mass flow rates, W_{Ls} and W_{Lus}, of the separated liquid and the unseparated liquid at the exit were measured using a timer and graduated cylinders. Each measurement was conducted for 50 **sec**. To make the uncertainty estimated at 95**%** confidence in the measured flow rates less than 3**%**. The ratio W_s* of the separated flow rate to the total liquid flow rate was used as an index of the separator performance and was calculated by

$$W_s^* = \frac{W_{Ls}}{W_{Ls} + W_{Lus}} \tag{1}$$

The film thickness δ was measured using a laser focus displacement meter (LFD, LT-9030, Keyence, Ltd.). The applicability of LFD to film thickness measurements has been discussed elsewhere in detail by Takamasa and Hazuku[8]. The sampling period was 0.64 **msec**. and the measurement time was 32 **sec**. The sampling number was 50,000 points, which was large enough to obtain an accurate time-averaged film thickness δ_{mean}. The uncertainty in the measured δ was 0.65**%** [9] estimated at 95**%** confidence levels.

3 Results and discussion

3.1 Flow visualization

Recorded images of flow patterns at J_L = 0.080 **m/s** are shown in Fig. 5. The flow pattern transits from churn flow to annular flow as J_G increases. Under churn flow conditions (J_G = 8.0 **m/s**), the liquid film intermittently falls down along the barrel wall (the area of film designated by the red arrow in Fig. 5 shows an instance of such collapse), whereas the film continuously flows upward under annular flow conditions (J_G = 14.6, 24.1 **m/s**). In the latter case, detachment of the liquid film from the wall occurs at the downstream edge of the simulated POR (red circles in Fig. 5) and the detached area increases with J_G. A part of the detached liquid film is entrained in the gas core flow as droplets, and the residual of the separated liquid film reattaches to the barrel wall to rejoin the liquid film. The entrained droplets deposit on the liquid film downstream of the simulated POR (white circles in Fig. 5).

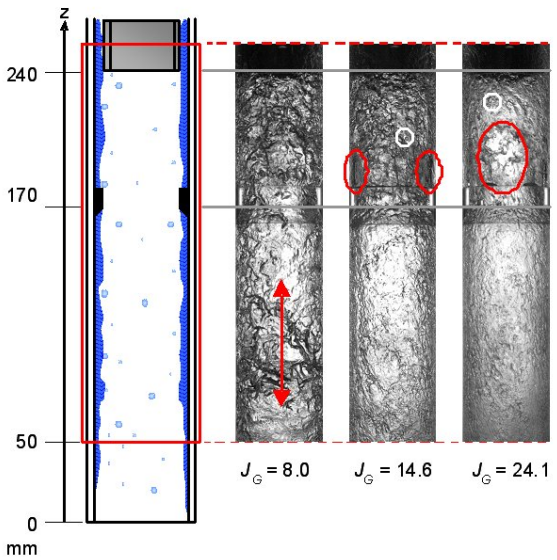

Fig. 5 Flow pattern in the barrel (J_L = 0.080 **m/s**).

Recorded images of flow patterns at J_G = 14.6 **m/s** are shown in Fig. 6. The flow pattern in each condition is annular flow irrespective of J_L. The areas of detached film (red circles in Fig. 6) decrease in size as J_L decreases and water accumulates just behind the simulated POR at low J_L (blue circle in Fig. 6). The entrainment of droplets at the rear edge of the simulated POR decreases with J_L, and therefore, the deposition of droplets on the liquid film (white circles in Fig. 6) also decreases with J_L.

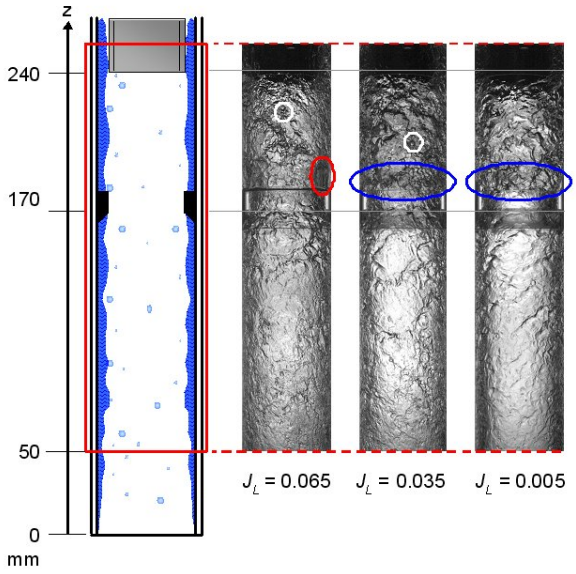

Fig. 6 Flow pattern in the barrel (J_G = 14.6 **m/s**).

Figure 7 shows flow patterns inside the barrel which were recorded using a bore scope (R080-084-000-50, Olympus Corp.) mounted on a high-speed video camera. At high liquid volume flux, J_L = 0.065 **m/s**, a large number of droplets are entrained behind the simulated POR, while the number of droplets in the barrel decreases with increasing J_G. This is because the amount of droplet deposition on the liquid film increases due to the large centrifugal force at high J_G. By contrast, at low liquid volume flux, J_L = 0.005 **m/s**, droplet entrainment into the gas core is not observed clearly, and only a few droplets present in the gas core. Under all the flow rate conditions, swirling motion of waves on the film is observed even in the downstream region of the simulated POR.

3.2 Film thickness

Time-series data of instantaneous liquid film thickness δ in the downstream region of the simulated POR were obtained using the LFD. The inner pipe simulating the second POR was removed in the LFD measurements in order to understand the development of the liquid film thickness near the second POR. The mean film thickness δ_{mean} and the maximum film thickness δ_{max} were defined as the arithmetic average of δ and the value of film thickness at which the cumulative distribution function of δ was 99 **%**, respectively.

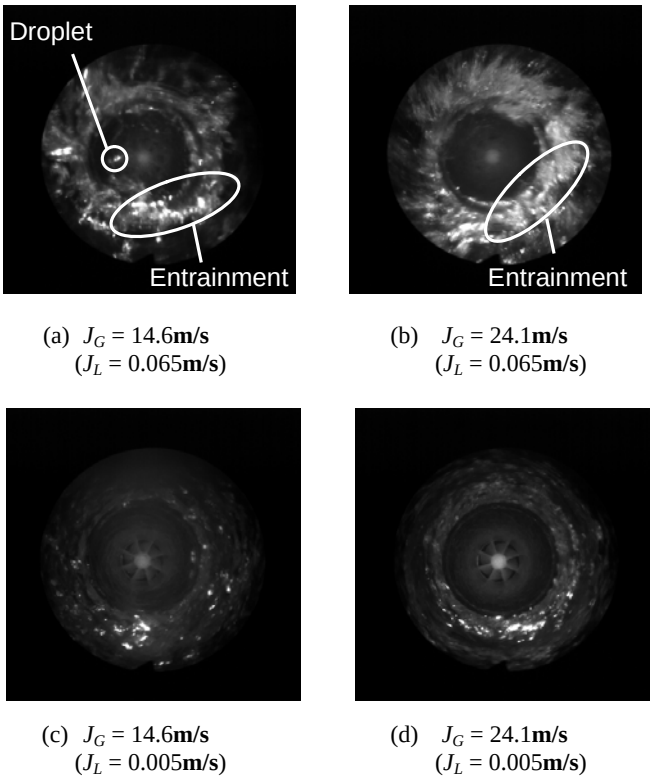

(a) J_G = 14.6**m/s** (J_L = 0.065**m/s**)

(b) J_G = 24.1**m/s** (J_L = 0.065**m/s**)

(c) J_G = 14.6**m/s** (J_L = 0.005**m/s**)

(d) J_G = 24.1**m/s** (J_L = 0.005**m/s**)

Fig. 7 Images of flow in the barrel (z = 240 **mm**).

Figure 8 shows the axial distributions of δ_{mean} and δ_{max} at J_G = 14.6 **m/s**. At low liquid volume fluxes (J_L = 0.005 – 0.035 **m/s**), the mean liquid film thickness behind the simulated POR is large and δ_{mean} gradually decreases in the direction of flow. This indicates that water accumulates just behind the simulated POR as shown in Fig. 9 (a) and that droplet entrainment is not significant at the downstream edge of the simulated POR. The liquid film is accelerated due to the interfacial shear force and becomes thinner as it flows downstream.

Under high liquid volume flux conditions (J_L = 0.065, 0.080 **m/s**), the mean liquid film thickness behind the simulated POR is small and gradually increases with elevation from base of the barrel. This indicates that the liquid film detaches and many droplets are entrained into the gas core at the downstream edge of the simulated POR as shown in Fig. 9 (b). Droplets deposit on the liquid film by centrifugal force, and the liquid film becomes thicker in the downstream region of the simulated POR.

The liquid film thickness just behind the simulated POR decreases with increasing J_L. This means that the

amount of droplet entrainment at the downstream edge of the simulated POR increases with J_L.

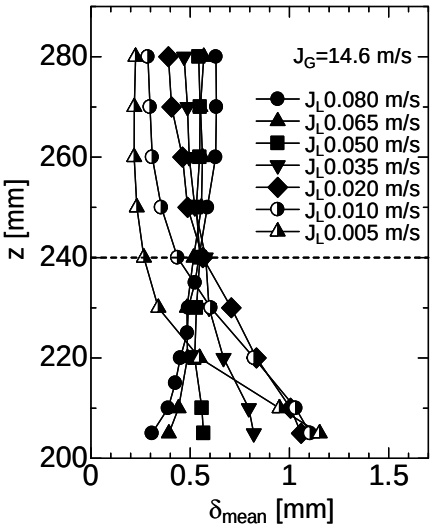

(a) Mean liquid film thickness

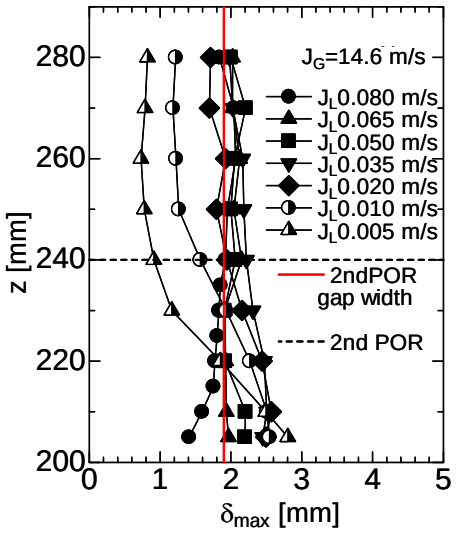

(b) The maximum liquid film thickness

Fig. 8 Mean and maximum liquid film thick nesses (J_G = 14.6 **m/s**).

Although the maximum liquid film thickness has the same trend as the mean film thickness, the changes in the maximum film thickness are smaller than those in the mean film thickness - except at low J_L. The maximum liquid film thickness is larger than the gap width of the second POR at the elevation of the second POR (z = 240 **mm**) in the case of $J_L \geq$ 0.035 **m/s**.

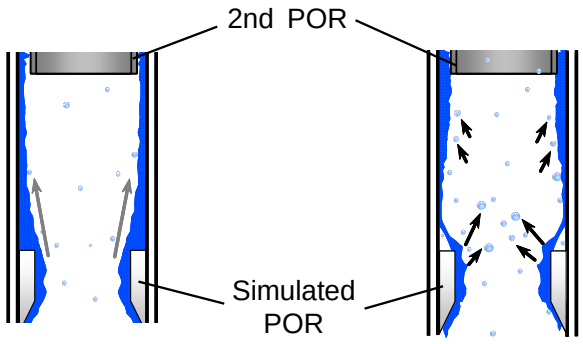

(a) Low J_L case (b) High J_L case

Fig. 9 Schematic of flow pattern around the simulated POR.

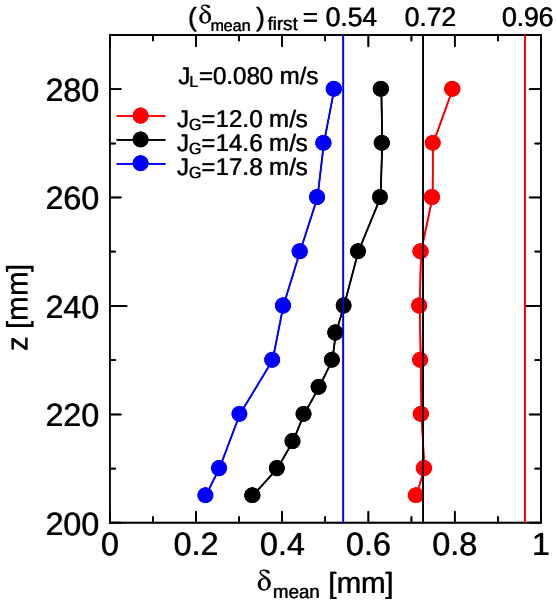

Fig. 10 Effects of J_G on mean liquid film thickness (J_L = 0.080 **m/s**).

Figure 10 shows the effects of J_G on the mean liquid film thickness at J_L = 0.080 **m/s**. The mean liquid film thickness decreases with increasing J_G. This is obviously due to the increase in interfacial friction. The vertical lines in Fig. 10 show the mean liquid film thickness $(\delta_{mean})_{first}$ at the position of the first POR (z = 170 **mm**) in the barrel without the simulated POR. Hence, the difference between $(\delta_{mean})_{first}$ and δ_{mean} indicates the effect of the presence of the simulated POR on the film thickness. Since δ_{mean} is smaller than $(\delta_{mean})_{first}$, the simulated POR reduces the liquid film thickness due to droplet entrainment at the rear edge of the POR. The δ_{mean} increases with z due to droplet deposition on the liquid film and approaches $(\delta_{mean})_{first}$. The difference between $(\delta_{mean})_{first}$ and δ_{mean} at the elevation of the second POR (z = 240 **mm**) decreases with increasing J_G. This is because centrifugal force in the downstream region of the

simulated POR increases with J_G, so that the amount of droplet deposition on the liquid film increases with J_G.

3.3 Flow separation

Figure 11 shows the measured W_s*. At high liquid volume fluxes (J_L = 0.035 – 0.065 **m/s**) and low gas volume fluxes (J_G = 12.0 – 17.8 **m/s**), J_L does not affect W_s* significantly due to the weak dependence of δ_{max} and δ_{mean} on J_L at the elevation of the second POR as shown in Fig. 8. By contrast, J_L affects W_s* at high gas volume fluxes ($J_G \geq$ 21.0 **m/s**), at which a large number of droplets are entrained at the rear edge of the simulated POR, and therefore, some droplets do not deposit on the liquid film and are retained in the gas core at the elevation of the second POR at high J_L. Hence, W_s* decreases with increasing J_L.

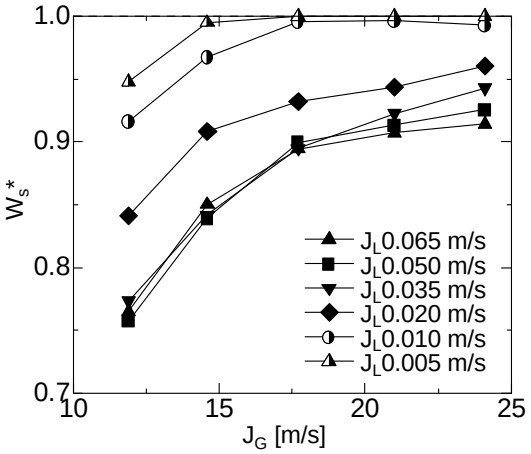

Fig. 11 Effects of J_L on W_s*.

At low liquid volume fluxes (J_L = 0.005, 0.010 **m/s**), W_s* is higher than that at high liquid volume fluxes. This is because the maximum liquid film thickness δ_{max} is smaller than the gap width of the second POR. Since W_s* is 1.0 at J_G = 17.8 – 24.1 **m/s** and J_L = 0.005 **m/s**, few droplets exist in the gas core under these conditions. This result is consistent with the visualized image of the flow shown in Fig. 7 (d).

W_s* is higher at J_L = 0.020 **m/s** than at J_L = 0.035 – 0.065 **m/s**, although the difference in the maximum liquid film thickness δ_{max} among these conditions is small. This indicates that the amount of droplets entrained in the gas core is smaller at J_L = 0.020 **m/s** than at J_L = 0.035 – 0.065 **m/s**. This is also obvious from the fact that the mean liquid film thickness at J_L = 0.020 **m/s** decreases as z increases as shown in Fig. 8, whereas δ_{mean} is almost constant or increases with z in the higher J_L cases.

4 Improvement of POR

We confirmed in the previous section that the droplet entrainment is large at the rear edge of the simulated POR, especially under high liquid volume flux conditions. The separation performance of the second POR is degraded due to droplet entrainment. Hence, the suppression of droplet entrainment at the first POR may increase the separation performance of the second POR. An improved simulated POR, which has a sloping tail as shown in Fig. 12, was installed in the barrel and the separation performance of the second POR was measured to examine the effect of the improvement. The angle of the slope was 7 degrees, which was determined by referring to angles of diffusers having no flow separation in single phase flows [10].

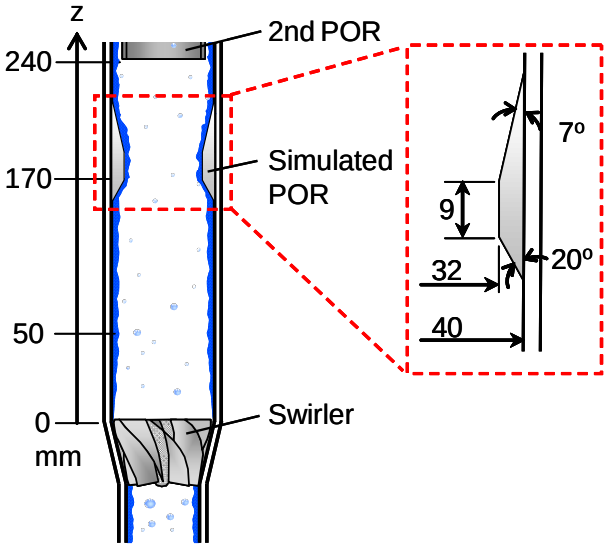

Fig. 12 Improved simulated POR.

Figure 13 shows comparisons of W_s* between the normal and improved PORs. At high liquid volume fluxes (J_L = 0.020 – 0.065 **m/s**), W_s* is significantly improved by the improved POR. The condition of J_G = 14.6 and J_L = 0.035 **m/s** is close to the normal operating conditions of practical separators. W_s* in these conditions is improved from 0.84 to 0.90. On the other hand, the effect of improvement on W_s* is small at low liquid volume fluxes (J_L = 0.005, 0.010 **m/s**). This is because that the amount of droplet

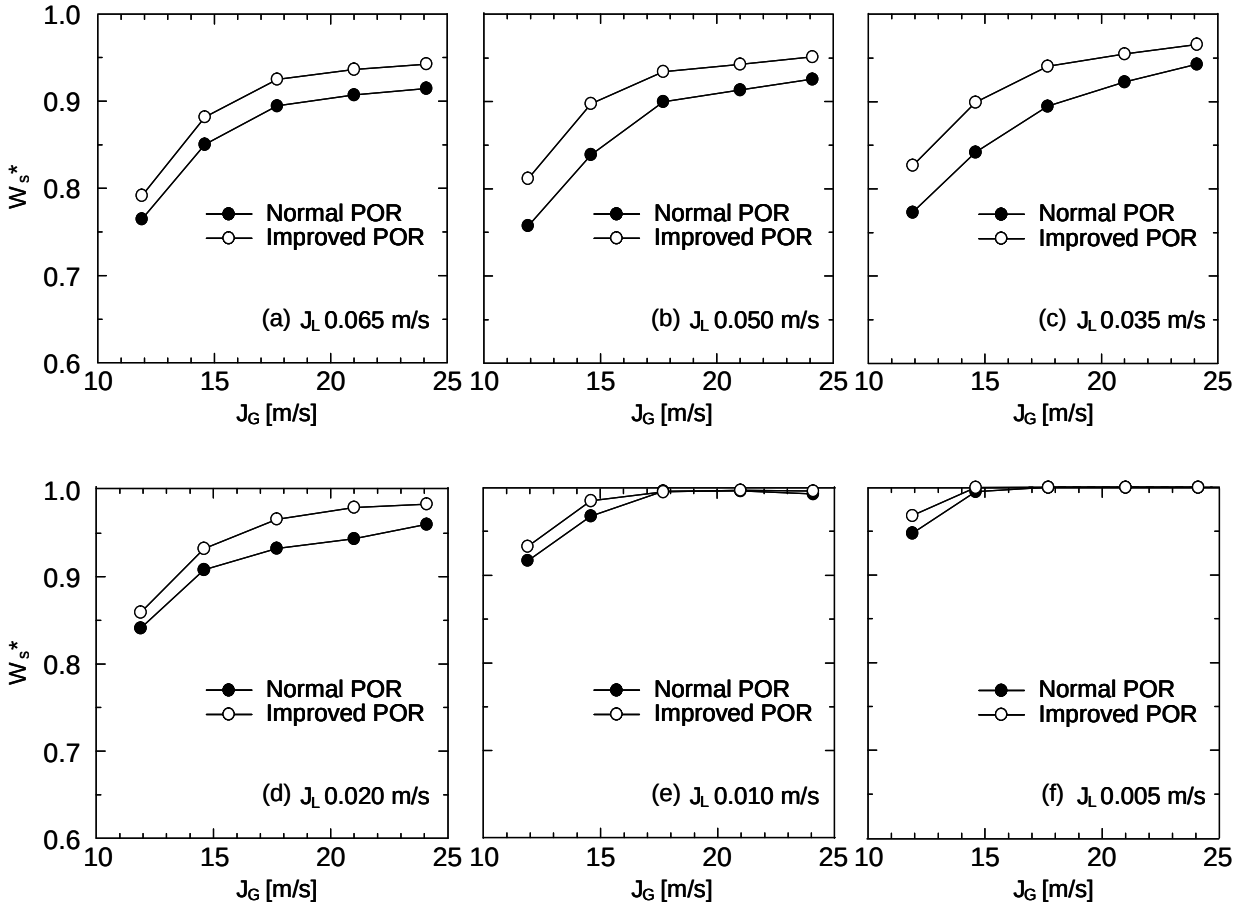

Fig. 13 Effect of POR shape on W_s*.

entrainment is small even for the normal POR. For all the flow rate conditions, the suppression of the droplet entrainment at the rear edge of the first POR by using a sloping tail is effective for improving separation performance at the second POR.

5 Conclusions

Characteristics of swirling flow after passing through the first POR were experimentally investigated using a downscaled model of a steam separator in which a simulated POR was installed. Flow patterns, liquid film thickness and separation performance at the second POR were measured. An improved POR, which had a sloping tail for suppressing droplet entrainment at the tail of the first POR, was installed and effects of the tail shape on the separation performance at the second POR were examined. As a result, the following conclusions were obtained:

(1) At high liquid volume fluxes, the liquid film separated from the wall and many droplets became entrained in the gas core at the downstream edge of the simulated POR. The liquid film thickness above the POR gradually increased due to droplet deposition induced by centrifugal force.

(2) At low liquid volume fluxes, water accumulated just behind the simulated POR, and the film thickness decreased in the flow direction due to the acceleration of the liquid by interfacial shear force.

(3) The suppression of droplet entrainment at the rear edge of the first POR by using a sloping tail is effective for improving separation performance at the second POR especially at high liquid volume fluxes.

Nomenclature

D:	Diameter	[**m**]
J_G:	Gas volume flux	[**m/s**]
J_L:	Liquid volume flux	[**m/s**]
L:	Length	[**m**]
W_{LS}:	Mass flow rate of separated liquid	[$\mathbf{m^3/s}$]
W_{LUS}:	Mass flow rate of unseparated liquid	[$\mathbf{m^3/s}$]
W_s*:	Ratio of separated flow rate to total flow rate	
z:	Elevation from barrel inlet	[**m**]
δ_{max}:	The maximum liquid film thickness	[**m**]
δ_{mean}:	Mean liquid film thickness	[**m**]
$(\delta_{mean})_{first}$:	Mean liquid film thickness at the first POR	[**m**]

Acknowledgments

The authors would like to thank Mr. Kenichi Katano and Dr. Koji Nishida (Hitachi, Ltd.) for their support with the present experiments.

References

[1] NAKAO, T., MURASE, M., ISHIDA, N., KAWAMURA, T., MINATO, A., and MORIYA, K.: Decrease of Pressure Loss in BWR Steam Separator (1) (Evaluation Method of Gas-Liquid Separation), Japanese Journal of Multiphase Flow, 2001, 15(4): 382-389. (In Japanese)

[2] IKEDA, H., SHIMIZU, T., NARABAYASHI, T., KONDO, T., NISHIDA, K., and FUKUDA, T.: Improvement of BWR Steam Separator with Three-Dimensional Gas-Liquid Two-Phase Flow Simulation Method, Proceedings of the 11th International Conference on Nuclear Engineering (ICONE-11), 2003, Paper No. 36486: 1-9.

[3] KATAOKA, H., TOMIYAMA, A., HOSOKAWA, S., SOU, A., and CHAKI, M.: Two-Phase Swirling Flow in a Gas-Liquid Separator, Journal of Power and Energy Systems, 2008, 2(4): 1120-1131.

[4] KATAOKA, H., TOMIYAMA, A., HOSOKAWA, S., SOU, A., and CHAKI, M.: Swirling Annular Flow in a Steam Separator, Journal of Engineering of Gas Turbines and Power, 2009, 131: 1-7.

[5] KATAOKA, H., TOMIYAMA, A., HOSOKAWA, S., SOU, A., and CHAKI, M.: Effects of Pick-off-Ring Configuration on Separation Performance of Gas-Liquid Separator, Progress in Multiphase Flow Research, 2007: 67-74. (In Japanese)

[6] KATAOKA, H., SHINKAI, Y., and TOMIYAMA, A.: Effects of Swirler Shape on Two-Phase Swirling Flow in a Steam Separator, Journal of Power and Energy Systems, 2009, 3(2): 347-355.

[7] MISHIMA, K., TOMIYAMA, A., OKAWA, T., TAKEUCHI, H., KUDO, Y., YAMAMOTO, Y., and CHAKI, M.: Research on ABWR Plants of Hyper Core Power Density, Proceedings of the 11th National Symposium on Power and Energy Systems (SPES 2006), 2006, 11: 225-230. (in Japanese)

[8] TAKAMASA, T., and HAZUKU, T.: Measuring a Film Flowing Down a Vertical Wall Using Laser Focus Displacement Meters (1st Report, Measuring Principle and Film Thickness), Transactions of the Japan Society of Mechanical Engineers, Series B, 1998, 64(617): 128-135. (In Japanese)

[9] KATAOKA, H., SHINKAI, Y., and TOMIYAMA, A.: Pressure Drop in Two-Phase Swirling Flow in a Steam Separator, Journal of Power and Energy Systems, 2009, 3(2): 382-392.

[10] JSME Data Book, Hydraulic Losses in Pipes and Ducts, 1993. (In Japanese)